Macroscopic scaling of high-order harmonics generated by two-color optimized waveforms in a hollow waveguide

Cheng Jin,[1,*] Kyung-Han Hong,[2] and C. D. Lin[3]

[1]*Department of Applied Physics, Nanjing University of Science and Technology, Nanjing, Jiangsu 210094, People's Republic of China*
[2]*Department of Electrical Engineering and Computer Science and Research Laboratory of Electronics,
Massachusetts Institute of Technology (MIT), Cambridge, Massachusetts 02139, USA*
[3]*J. R. Macdonald Laboratory, Department of Physics, Kansas State University, Manhattan, Kansas 66506, USA*

We present the macroscopic scaling of high harmonics generated by two-color laser pulses interacting with Ne gas in a hollow waveguide. We demonstrate that the divergence of harmonics is inversely proportional to the waveguide radius and harmonic yields are proportional to the square of the waveguide radius when the gas pressure and waveguide length are chosen to meet the phase-matching condition. We also show that harmonic yields are inversely proportional to the ionization level of the optimized two-color waveform with proper gas pressure if waveguide radius and length are fixed. These scaling relations would help experimentalists find phase-matching conditions to efficiently generate tabletop high-flux coherent soft x rays for applications.

I. INTRODUCTION

High-order harmonics generated in a gas medium by an intense ultrafast laser would provide tabletop light sources extending from extreme ultraviolet (XUV) to x rays on the femtosecond or even attosecond time scale [1,2]. Because of their excellent spatial and temporal coherence properties, high-harmonic light sources have been widely applied in different research areas of physics and chemistry [3], from the probing of ultrafast electronic processes [4,5] to ultrahigh precision measurement of narrow XUV transitions [6], imaging of nanoscale structure [7], and so on. High-order harmonic generation (HHG) is a highly nonlinear process which is sensitive to the driving laser and the gas target [8–11]. Therefore, there is a wide range of macroscopic parameters that affects the generation of harmonics in an experiment, thus making it difficult to locate the needed phase-matching conditions for the efficient buildup of macroscopic harmonic fields in a gas medium [12–14].

The available laser systems in different laboratories are varied. For applications HHG sources in different spectral or intensity regions may be needed. It is advantageous to investigate the scaling of harmonic generation processes to extend existing macroscopic parameter space for reaching phase-matching conditions in new regimes [14,15]. One of the well studied examples is the scaling of HHG yield with the driving laser wavelength. By employing longer wavelength lasers [16–18], the cutoff energy of high harmonics increases quadratically with λ, but the single-atom harmonic yield scales like $\lambda^{-5 \sim -6}$ [19–23], where λ is the laser wavelength. On the other hand, the rapid decrease of harmonic yield at longer wavelength can be compensated by adjusting the macroscopic conditions, for example, by increasing the gas pressure [24,25]. Midorikawa's group investigated the power scaling of HHG using a self-guided beam in 2002 [26]. However, their designed scaling was not achieved due to the limitation in pulse energy. Recently, a general scaling rule has been proposed [14,27,28],

which identifies the invariance of HHG processes from the μJ-level multi-MHz high-repetition-rate lasers with tightly focused geometry to the loosely focused 100 mJ or Joule level pulses [29]. To obtain such scaling for nonlinear optical phenomena in gases [30], several macroscopic parameters, such as the medium length, beam diameter, focal length, and gas density, need to be appropriately scaled with input pulse energy. Scaling with macroscopic parameters embodied in the different generation geometries of strong-field phenomena will simplify the search of the phase-matching domain when exploring new regimes of HHG.

To overcome low up-conversion efficiency of HHG, it has been proposed to modify the subcycle laser waveform by optimally synthesizing multicolor laser pulses [31–37] (see review in Ref. [38]). We also suggested to include the influence of propagation effects in the optimization procedure for two-color waveforms, which were capable of enhancing soft x-ray harmonics by one to two orders over single-color laser pulses without the increase of the total power [39]. We then showed that low-divergence bright soft x-ray harmonics and isolated attosecond pulses were efficiently generated by guiding optimized two-color waveforms in a hollow waveguide while macroscopic parameters, such as gas pressure, waveguide radius and length, were further optimized [40,41]. However, it is still quite time consuming to routinely run propagation simulations, even in a reduced parameter space in which the most important macroscopic parameters are varied for a given optical waveform. Thus it is desirable to search for the scaling rule of high harmonics generated in a guided geometry [42–44]. So far the scaling of macroscopic parameters has been studied for one-color laser pulses in the free geometry only [14,26–28,30]. Whether or not such scaling will work for multicolor laser pulses in a hollow waveguide has not been examined yet.

The main goal of this article is to analyze how to properly scale high harmonics generated by two-color waveforms incident into a gas-filled hollow waveguide. We will identify the scaling rule for harmonic divergence [45–47] and harmonic yields with different parameters such as waveguide radius and ionization level. The article is arranged as follows: in

---
*Corresponding author: cjin@njust.edu.cn

Sec. II, we will briefly summarize the theoretical models for optimized waveforms, laser and HHG propagation, and far-field harmonic emission. In Sec. III, we will illustrate the scaling law of the harmonic divergence and harmonic yields with the waveguide radius under different phase-matching conditions by simulating the evolution of the electric field along the propagation distance. In Sec. IV, the scaling law will be presented in terms of the ionization level of the waveform; the article will be concluded in Sec. V.

II. THEORETICAL METHODS

A. Optimized two-color waveforms

The two-color waveform in Ref. [39] consists of a fundamental laser (with longer wavelength of λ_1) and its third harmonic (λ_2). In one optical cycle of the fundamental the electric field is expressed as

$$E(t) = E_1 \cos(\omega_1 t + \phi_1) + E_2 \cos(\omega_2 t + \phi_2). \quad (1)$$

Here E_i, ω_i, and ϕ_i ($i = 1, 2$) are the respective amplitudes, angular frequencies, and phases of the two pulses. In the optimization, ω_1 was given, ϕ_1 was set to zero for simplicity, and $\omega_2 = 3\omega_1$ since the third harmonic is the best in the two-color synthesis as demonstrated in Ref. [39]. We searched the parameters $\{E_1, E_2, \phi_2\}$ to maximize the single-atom HHG yield. Genetic algorithm (GA) was used to optimize the fitness function which is the maximal harmonic yield at the cutoff. Additional constraints that would favor single-atom harmonics after macroscopic propagation were imposed: (a) the cutoff energy should be maintained at the desired value; (b) in the plateau region, harmonic emissions from "short"-trajectory electrons should be stronger than those from the "long" ones; (c) the ionization level at the end of a single-cycle waveform was restricted to less than a predetermined value of a few percent. Examples of two-color optimized waveforms with different ionization level are shown in Table I.

B. Propagation of driving laser and harmonic fields in a hollow waveguide

To calculate XUV or soft x-ray high harmonics emitted in a gas-filled hollow waveguide, both time-dependent Schrödinger equations (TDSEs) and Maxwell's wave equations (MWEs) are solved. The former accounts for single-atom response to the laser pulse, and is calculated using the quantitative rescattering (QRS) model [48]. The propagation of

TABLE I. Laser parameters for two-color waveforms with varied ionization level. These waveforms can generate single-atom HHG cutoff energy at 250 eV for Ne atom. Laser intensities ($|E_1|^2$ and $|E_2|^2$) are in units of 10^{14} W/cm^2. λ_1 is fixed at 1600 nm, $\phi_1 = 0$, and $\lambda_2 = \lambda_1/3$. Taken from Supplementary Table 3 in Ref. [39].

Ionization level	$|E_1|^2$	$|E_2|^2$	ϕ_2
1%	2.39	0.50	1.50π
2%	1.98	1.32	1.36π
3%	1.98	1.40	1.43π
4%	1.95	1.55	1.46π
5%	1.84	1.88	1.42π

the laser pulses and harmonics in the macroscopic gas medium is calculated using the prescription in Ref. [49]. Further details of solving these propagation equations in a guided geometry were presented in Refs. [40,41].

In the simulation, the distribution of the gas density inside the waveguide is uniform. The initial spatial beams are chosen to be the lowest EH_{11} mode which can be obtained when the ratio between the beam waist of incident Gaussian pulse and the waveguide radius is about 65% [24]. Both colors are assumed to have a realistic Gaussian temporal envelope with full width at half maximum (FWHM) duration of 16 fs (three optical cycles of the 1.6 μm laser). The initial on-axis electric field at the entrance of the waveguide is always chosen to be the optimized two-color waveform. Near-field harmonics are taken to be the harmonics emitted on the exit plane of the hollow waveguide.

C. Far-field harmonic emission

To obtain the harmonic emission (or harmonic divergence) in the far field, near-field harmonics need to further propagate in the vacuum. In the paraxial approximation, far-field harmonics can be calculated through a Hankel transformation [49]

$$E_h^f(r_f, z_f, \omega) = ik \int_0^a \frac{E_h^n(r, z_n, \omega)}{z_f - z_n} J_0\left(\frac{krr_f}{z_f - z_n}\right)$$
$$\times \exp\left[-\frac{ik(r^2 + r_f^2)}{2(z_f - z_n)}\right] r \, dr, \quad (2)$$

where J_0 is the zeroth-order Bessel function, the wave vector k is given by $k = \omega/c$ with the harmonic frequency ω, and a is the waveguide radius. In Eq. (2), the positions of near and far fields are given by z_n and z_f, respectively. $E_h^n(r, z_n, \omega)$ is the near-field harmonic; r and r_f are the transverse coordinates in the near and far fields, respectively.

III. SCALING OF THE DIVERGENCE AND YIELD OF HARMONICS WITH THE WAVEGUIDE RADIUS

Previously, we have applied the waveform (WF) consisting of the 1.6 and 0.533 μm laser pulses at the 2% ionization level (see Table I) into a Ne gas-filled waveguide which has a radius of 125 μm to generate soft x-ray high harmonics. We varied both the waveguide length and the gas pressure, and found that the optimal values were 5 mm and 50 Torr, in order to achieve the highest cutoff energy of about 250 eV and the highest harmonic yields, simultaneously. The resulting harmonics are shown in Fig. 1(b). These harmonics have very good spatial coherence, and their half-divergence angles are within 1 mrad. We consider good phase matching has been achieved in this case.

To maintain the same phase matching, the waveguide radius, gas pressure, and medium length should be adjusted concurrently, instead of independently, i.e., the scaling of these parameters has to be identified. Since we are dealing with two-color laser pulses, the commonly used formulation of phase mismatch between the one-color laser pulse and high harmonics cannot be employed. Thus we turn to investigate the time shift for each color, using an analysis similar to Ref. [40].
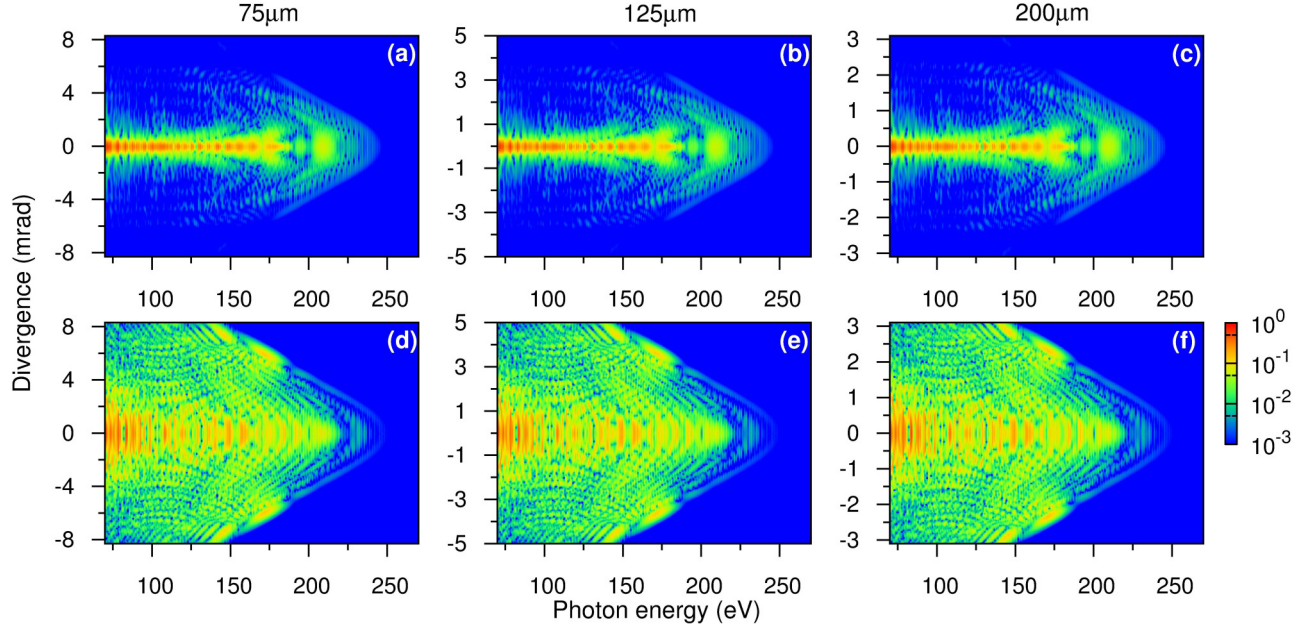
FIG. 1. Harmonic emission (normalized) in the far field using the two-color waveform with 2% ionization level in Table I as the initial on-axis laser pulse. The incident beam size is adjusted to ensure that the fundamental EH_{11} mode is guided. Other parameters for (a)–(f) are listed in Table II.

For each color, the refractive index inside the waveguide is expressed as

$$n_l \approx 1 - \frac{\mu_1^2 \lambda_l^2}{8\pi^2 a^2} + p(1-\eta)\delta_1(\lambda_l) - \frac{p\eta n_0 r_e \lambda_l^2}{2\pi}. \quad (3)$$

Here a is again the waveguide radius, μ_1 the mode factor ($=2.405$ for fundamental EH_{11} mode), p the gas pressure, η the ionization probability, λ_l the laser wavelength, δ_l the atomic dispersion, n_0 the neutral atomic density, and r_e the classical electron radius. Each correction term on the right-hand side of Eq. (3) contributes to the time shift (or group delay) with respect to the reference frame (moving at the speed of light). If the laser pulse has propagated a distance Δz, the time shift of each color due to the waveguide mode, the atomic dispersion, and the plasma defocusing can be respectively calculated from (see Supplemental Material in Ref. [40])

$$\Delta t_m = (\Delta z/c)\left(\mu_1^2 \lambda_l^2 / 8\pi^2 a^2\right), \quad (4)$$

$$\Delta t_a = (\Delta z/c) p[1 - \eta(t)]\delta_1(\lambda_l), \quad (5)$$

TABLE II. Macroscopic parameters for harmonic emissions in Fig. 1.

	Waveguide radius (μm)	Gas pressure (Torr)	Waveguide length (mm)
(a)	75	138.9	1.8
(b)	125	50.0	5.0
(c)	200	19.5	12.8
(d)	75	55.6	1.4
(e)	125	20.0	4.0
(f)	200	7.8	10.2

and

$$\Delta t_p = (\Delta z/c)\left[p\eta(t)n_0 r_e \lambda_l^2 / 2\pi\right]. \quad (6)$$

Here the ionization probability $\eta(t)$ has time dependence, and its value at the end of the laser pulse is defined as the ionization level.

As demonstrated in Ref. [40], the two-color waveform after propagation obtained by numerically solving the MWEs can be made to phase match, by properly shifting the depleted (or designed) waveform with respect to the reference frame, with each of the time shifts calculated using Eqs. (4)–(6), including contributions from both colors. If the time shifts in these equations are kept the same, the evolution of the two-color laser pulse inside the waveguide will not change, thus leading to invariant phase matching.

If one varies the waveguide radius only, to maintain the same time shift the propagation distance Δz in Eq. (4), or the waveguide length, should be scaled by a^2. To keep the same time shifts in Eqs. (5) and (6), gas pressure p should be inversely proportional to Δz, i.e., $\propto 1/a^2$. Thus in Table II we choose two waveguide radii of 75 and 200 μm in (a) and (c), as compared to the previous one at 125 μm in (b), and the gas pressure and waveguide length are also properly scaled as just discussed with respect to the values in (b). By using the same 2% ionization waveform as the initial on-axis laser pulse, the simulated harmonic spectra are shown in Figs. 1(a) and 1(c). We can see that harmonic spectra (after normalization) in these two figures are the same as that in Fig. 1(b), except that the angular divergence has been rescaled. We have checked that the normalization factor of the harmonics is proportional to a^4, and half-divergence angle is actually proportional to $1/a$. The total harmonic yields integrated over the radial distance are shown in Fig. 2(a). The shape of the harmonic spectra obtained from the three waveguide radii looks the same and the harmonic
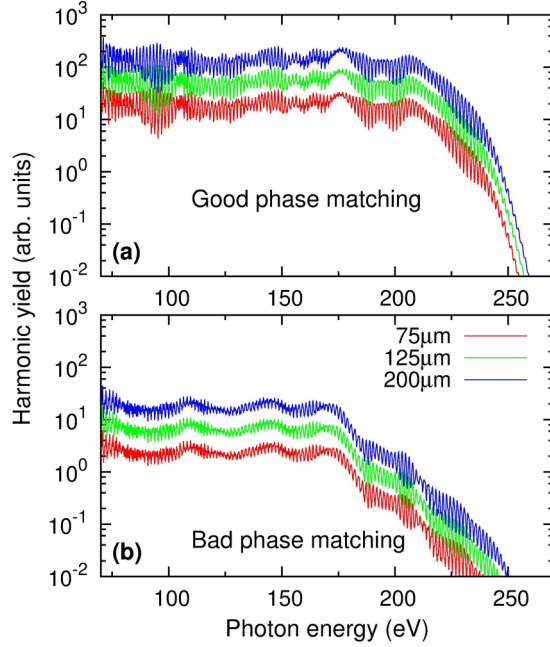
FIG. 2. Total harmonic yields integrated over the radial distance for (a) good and (b) bad phase-matching conditions. Panels (a) and (b) correspond to harmonic emissions in Figs. 1(a)–1(c) and in Figs. 1(d)–1(f), respectively. In both (a) and (b), from top to bottom, three curves are for waveguide radii of 200, 125, and 75 μm, respectively.

yields have been checked to be proportional to a^2. These results confirm the scaling of HHG driven by the two-color pulses in the waveguide if the macroscopic parameters are correctly scaled.

To understand how scaling works for the harmonic angular divergence and yield, we examine the spatiotemporal laser field in the reference frame at two selected waveguide positions, one at the middle and the other at the end, of the waveguide. In Figs. 3(a)–3(c), for the position at the middle, the field distributions are the same in the three figures except that the radial dimensions are different. The field distributions at the end of the waveguide, as shown in Figs. 3(d)–3(f), remain the same except that the field strength has decreased. These results show that based on the time shift analysis for two-color pulses, we have been able to establish the same spatial laser intensity distributions at appropriately scaled distances.

The scaling of angular divergence of the harmonics in the far field can be understood by using Fig. 3. A direct consequence of spatial scaling of the laser field with a is that the same scaling applies to the harmonics inside the waveguide. Thus the spatial distribution of near-field harmonics $E_h^n(r,z_n,\omega)$ in Eq. (2) also scales with a. In Eq. (2), the term $\exp[-ikr^2/2(z_f - z_n)]$ can be approximated as 1.0 since the effective r-integration region is pretty small such that $r^2 \ll (z_f - z_n)/k$ for soft x-ray harmonics and for far field located much further away from the exit of the waveguide. To maintain invariance of the term $J_0[krr_f/(z_f - z_n)]$, r_f should scale with $1/a$, i.e., harmonic divergence in the far field scales with $1/a$. After integration over r, which scales with a, far-field harmonic $E_h^f(r_f,z_f,\omega)$ at the scaled r_f is thus $\propto a^2$. This explains why the normalization factor in Figs. 1(a)–1(c) is proportional to a^4.

The scaling of the total harmonic yields can also be explained by using Fig. 3. The total harmonic yields can be calculated from

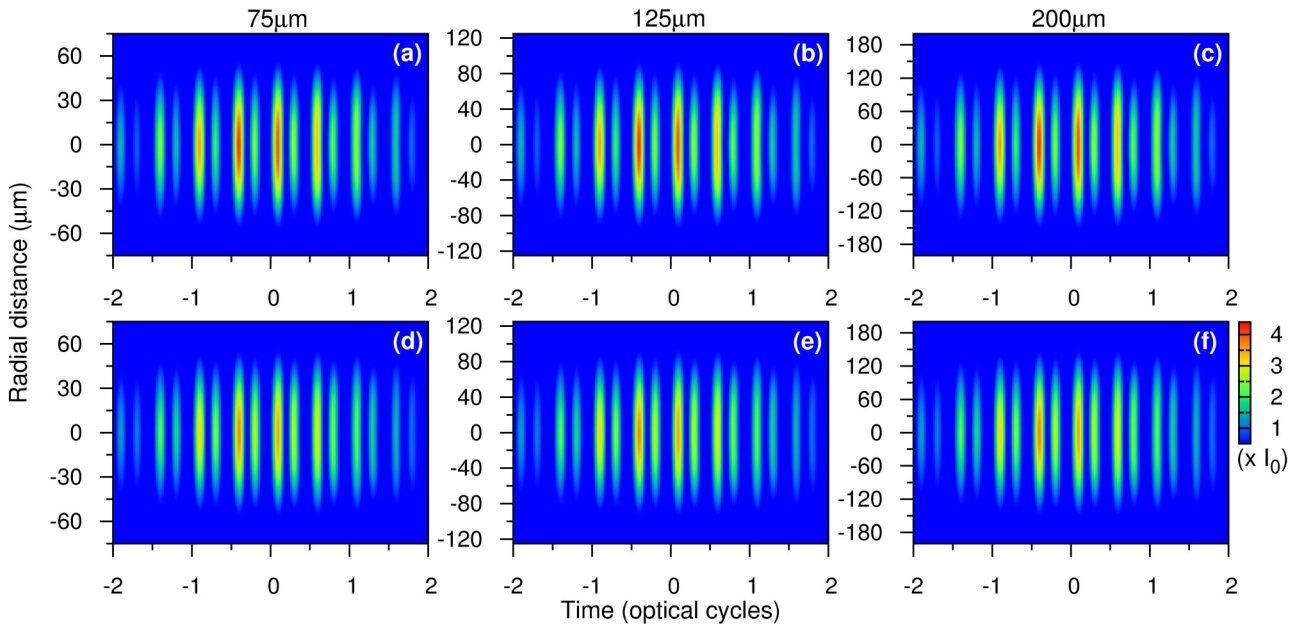$$S(\omega) \propto \int_0^a \left| E_h^n(r,z_n,\omega) \right|^2 r \, dr. \tag{7}$$

FIG. 3. Spatiotemporal laser intensity distributions of two-color 2% waveforms in the middle [(a)–(c)] and in the end [(d)–(f)] of gas medium for different waveguide radii as indicated. The propagation distances are 0.9, 2.5, and 6.4 mm in (a)–(c), and are 1.8, 5.0, and 12.8 mm in (d)–(f), respectively. Gas pressure and waveguide length are chosen from (a)–(c) in Table II. These laser fields induce harmonic emissions in Figs. 1(a)–1(c). I_0 is in the units of 10^{14} W/cm^2, and optical cycles are for the fundamental 1.6 μm laser.
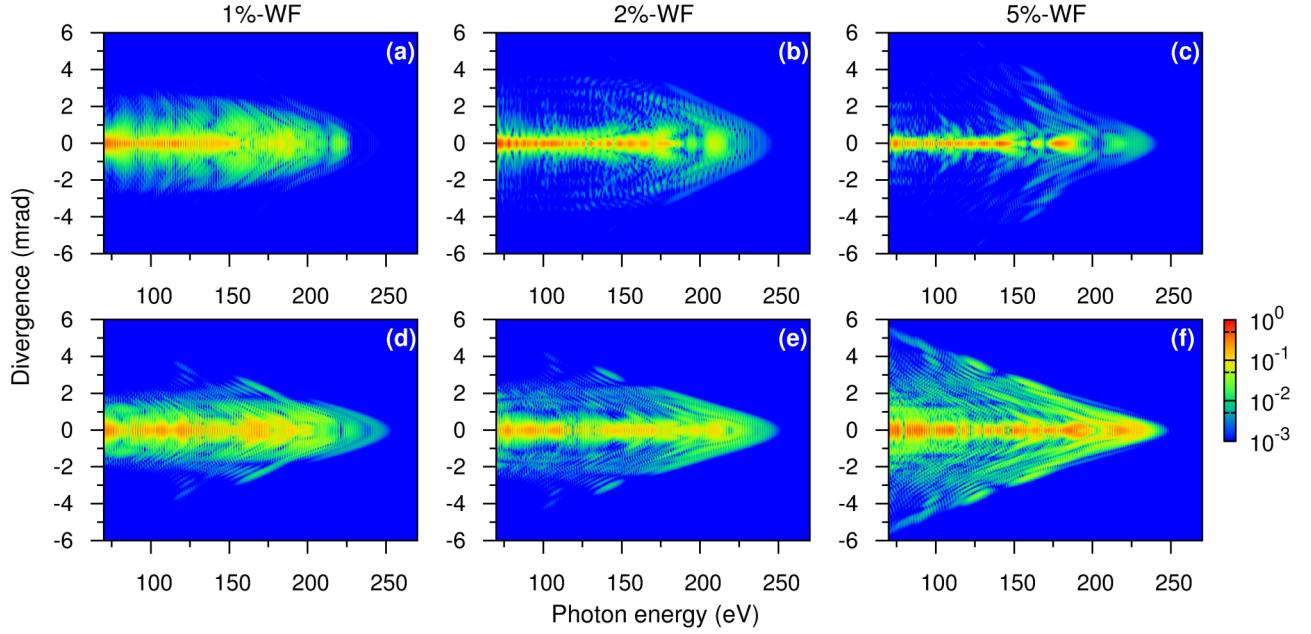
FIG. 4. Harmonic emissions in the far field by two-color waveforms at different ionization levels; see the waveform parameters in Table I. The incident beam sizes of the two colors are independently adjusted to ensure that the fundamental EH_{11} mode is guided. Waveguide radii and lengths are 125 μm and 5 mm in (a)–(c) and 200 μm and 7 mm in (d)–(f), respectively. Gas pressures are listed in Table III.

Since the spatial distribution of $|E_h^n(r,z_n,\omega)|^2$ along r scales with a, the integration in Eq. (7) is proportional to a^2, i.e., $S(\omega) \propto a^2$. This explains the observed scaling of total harmonic yields in Fig. 2. On the other hand, as discussed in Sec. II, the initial on-axis waveform is kept the same as the waveguide radius is varied; the input two-color laser pulse energy is thus proportional to a^2. So the harmonic conversion efficiency at different radii is not changed.

So far we only present examples of HHG under good phase-matching conditions. Is scaling applicable to harmonic generation under poor phase-matching conditions? We start with waveguide radius of 125 μm, and choose gas pressure of 20 Torr and medium length of 4 mm. The corresponding parameters for radii of 75 or 200 μm are listed in Table II to ensure that gas pressure is $\propto 1/a^2$ and waveguide length is $\propto a^2$. The simulated harmonic emissions in the far field are shown in Figs. 1(d)–1(f). The harmonic distributions for the three waveguide radii are the same, all with considerable on- and off-axis emissions, indicating poor phase matching during the propagation. The harmonic divergence is still proportional to $1/a$. The total harmonic yields are shown in Fig. 2(b), in which the cutoff energies are significantly reduced by about 50 eV. The features of harmonic spectra are the same, and harmonic yields are proportional to a^2. Since the input pulse energy is $\propto a^2$, the harmonic conversion efficiency is invariant when the waveguide radius is varied. These results show that the scaling law discovered at good phase-matching condition is also valid at unfavorable phase-matching condition.

IV. SCALING OF HARMONIC YIELD WITH WAVEFORM IONIZATION LEVEL

As discussed in Sec. II, changing the ionization level adds an additional freedom for laser waveform optimization. Is

it possible to remove the uncertainty of ionization level by identifying its best value when macroscopic conditions are taken into account? Starting with the HHG process by using the 2%-ionization waveform under the optimal conditions (gas pressure of 50 Torr and waveguide length of 5 mm) for the waveguide with the radius of 125 μm, the harmonic emissions are replotted in Fig. 4(b). If the ionization level η in the waveform is varied while the waveguide radius and length are fixed, the time shifts caused by dispersions in Eqs. (4)–(6) should not be changed in order to preserve phase matching. At low gas pressure we can neglect the time shift Δt_a due to atomic dispersion. Since the waveguide is the same there is no change of time shift from the waveguide mode. Thus to keep the same phase-matching condition, the time shift in Δt_p caused by the plasma should remain the same, by changing the gas pressure by a factor proportional to $1/\eta$. So if the waveguide is fixed, good phase matching is maintained by scaling the pressure by $1/\eta$ if the ionization level η is modified; see Table III. Figures 4(a) and 4(c) show the harmonic spectra by using waveform at ionization levels of 1% and 5% with scaled pressures; the well localized emissions along the axis in Fig. 4(b) are better maintained in Fig. 4(c) than in Fig. 4(a). Since the waveguide radius is fixed, the divergence of high harmonics is not changed among the three figures. The total

TABLE III. Gas pressures for HHG in Figs. 4 and 5 at two waveguide radii. Ionization levels of two-color waveforms are indicated.

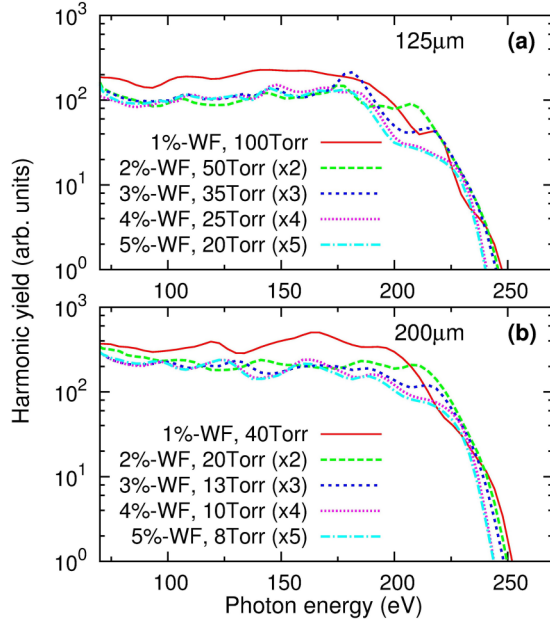| Radius (μm)	Gas pressure (Torr)				
	1%	2%	3%	4%	5%
125	100	50	35	25	20
200	40	20	13	10	8

FIG. 5. Total harmonic yields integrated over the radial plane for waveguide radius at (a) 125 μm and (b) 200 μm. Panels (a) and (b) are the integrated harmonic emissions in Figs. 4(a)–4(c) and in Figs. 4(d)–4(f), respectively. The harmonic spectra are smoothed by using Bezier curve for easy comparison, and the multiplied factors are indicated.

harmonic yields integrated over radial distance are shown in Fig. 5(a). Each harmonic spectrum has been multiplied by a factor that is proportional to η. The overlap of harmonic spectra for 2% to 5% WF indicates that harmonic yields are proportional to $1/\eta$. Exception occurs for the 1% WF because gas pressure is too high and approximations that lead to the neglect of Eq. (5) are no longer valid.

The scaling of harmonic yields with ionization level η can be easily understood. Since phase-matching conditions are maintained, total harmonic yields are proportional to p^2. On the other hand, single-atom harmonic yield is $\propto \eta$. Combining two factors, the total harmonic yield is $\propto 1/\eta$.

This scaling law has been tested for another example at the waveguide radius of 200 μm. The low-divergence harmonic emissions have been obtained in Ref. [40] by using 2% WF under optimal conditions (gas pressure of 20 Torr and waveguide length of 7 mm). The spectrum is replotted in Fig. 4(e). For other ionization levels the parameters are listed in Table III. The harmonic emissions and total harmonic yields are shown in Figs. 4(d)–4(f) and Fig. 5(b), respectively. The results are in agreement with the previous ones using 125 μm radius.

The scaling law tells us that 2% ionization can be considered as the best value since the divergence of harmonics in the far

field is better than the 1% WF, and harmonic yields are the strongest among other waveforms.

V. CONCLUSIONS

In summary, we investigated the scaling of the HHG process driven by two-color waveforms in a Ne gas-filled waveguide. Our simulations showed that the angular divergence of harmonics is inversely proportional to the waveguide radius, and the total harmonic yield is proportional to the square of the waveguide radius if gas pressure and waveguide length are chosen, respectively, to be inversely proportional and proportional to the square of waveguide radius. The analysis of the evolution of two-color driving laser pulses during the propagation in the waveguide allowed us to understand the physical mechanism of maintaining the phase-matching conditions by appropriately choosing macroscopic parameters. The conclusions of scaling are valid for both good and bad phase-matching conditions. We further showed that total harmonic yields are roughly inversely proportional to the ionization level when gas pressure is chosen to be inversely proportional to the ionization level for a hollow waveguide with fixed radius and length.

Our scaling results imply that a large number of routine, time-consuming macroscopic calculations can be efficiently reduced with fewer macroscopic parameters. To generate high-flux bright coherent soft x rays, it is preferable to focus laser beams with high pulse energy at the entrance of a large-bore hollow waveguide. However, we need to point out that some technical difficulties may prevent the realization of using a long straight hollow waveguide and for coupling with high energy laser pulses into a waveguide because of the increased fluctuations of beam pointing, and beyond a certain beam size, the waveguide may not be necessary. To optimize multicolor laser waveforms for HHG, it is very crucial to set ionization level under a few percent.

Similar scaling rules should apply to the generation of soft x-ray isolated attosecond pulses by using two-color waveforms consisting of the fundamental laser and its second harmonic in a hollow waveguide [41]. We anticipate this study to inspire further interest in studying macroscopic HHG scaling in other guided geometries, free geometries, or beam truncated geometries [50,51] by using single- or multicolor laser pulses.

[1] F. Krausz and M. Ivanov, Rev. Mod. Phys. **81**, 163 (2009).

[2] F. Calegari, G. Sansone, S. Stagira, C. Vozzi, and M. Nisoli, J. Phys. B **49**, 062001 (2016).

[3] L.-Y. Peng, W.-C. Jiang, J.-W. Geng, W.-H. Xiong, and Q. Gong, Phys. Rep. **575**, 1 (2015).

[4] F. Calegari *et al.*, Science **346**, 336 (2014).

[5] Y. Pertot *et al.*, Science **355**, 264 (2017).

[6] A. Cingöz, D. C. Yost, T. K. Allison, A. Ruehl, M. E. Fermann, I. Hartl, and J. Ye, Nature (London) **482**, 68 (2012).

[7] J. Miao, T. Ishikawa, I. K. Robinson, and M. M. Murnane, Science **348**, 530 (2015).

[8] V. Tosa, H. T. Kim, I. J. Kim, and C. H. Nam, Phys. Rev. A **71**, 063807 (2005).

[9] E. Priori, G. Cerullo, M. Nisoli, S. Stagira, S. De Silvestri, P. Villoresi, L. Poletto, P. Ceccherini, C. Altucci, R. Bruzzese, and C. de Lisio, Phys. Rev. A **61**, 063801 (2000).

[10] I. P. Christov, Phys. Rev. A **60**, 3244 (1999).

[11] F. Wang, L. He, C. Zhai, W. Shi, Q. Zhang, P. Lan, and P. Lu, Phys. Rev. A **92**, 063839 (2015)

[12] M. B. Gaarde, J. L. Tate, and K. J. Schafer, J. Phys. B **41**, 132001 (2008).

[13] V. S. Yakovlev, M. Ivanov, and F. Krausz, Opt. Express **15**, 15351 (2007).

[14] C. M. Heyl, C. L. Arnold, A. Couairon, and A. L'Huillier, J. Phys. B **50**, 013001 (2017).

[15] B. Shan and Z. Chang, Phys. Rev. A **65**, 011804 (2001).

[16] K.-H. Hong *et al.*, Opt. Lett. **39**, 3145 (2014).

[17] D. Sanchez, M. Hemmer, M. Baudisch, S. L. Cousin, K. Zawilski, P. Schunemann, O. Chalus, C. Simon-Boisson, and J. Biegert, Optica **3**, 147 (2016).

[18] Y. Yin, A. Chew, X. Ren, J. Li, Y. Wang, Y. Wu, and Z. Chang, Sci. Rep. **7**, 45794 (2017).

[19] J. Tate, T. Auguste, H. G. Muller, P. Salières, P. Agostini, and L. F. DiMauro, Phys. Rev. Lett. **98**, 013901 (2007).

[20] K. Schiessl, K. L. Ishikawa, E. Persson, and J. Burgdörfer, Phys. Rev. Lett. **99**, 253903 (2007).

[21] M. V. Frolov, N. L. Manakov, and A. F. Starace, Phys. Rev. Lett. **100**, 173001 (2008).

[22] A. D. Shiner, C. Trallero-Herrero, N. Kajumba, H.-C. Bandulet, D. Comtois, F. Légaré, M. Giguère, J.-C. Kieffer, P. B. Corkum, and D. M. Villeneuve, Phys. Rev. Lett. **103**, 073902 (2009).

[23] A. T. Le, H. Wei, C. Jin, V. N. Tuoc, T. Morishita, and C. D. Lin, Phys. Rev. Lett. **113**, 033001 (2014).

[24] T. Popmintchev, M.-C. Chen, A. Bahabad, M. Gerrity, P. Sidorenko, O. Cohen, I. P. Christov, M. M. Murnane, and H. C. Kapteyn, Proc. Natl. Acad. Sci. USA **106**, 10516 (2009).

[25] T. Popmintchev *et al.*, Science **336**, 1287 (2012).

[26] E. Takahashi, Y. Nabekawa, T. Otsuka, M. Obara, and K. Midorikawa, Phys. Rev. A **66**, 021802(R) (2002).

[27] C. M. Heyl, J. Güdde, A. L'Huillier, and U. Höfer, J. Phys. B **45**, 074020 (2012).

[28] J. Rothhardt, M. Krebs, S. Hädrich, S. Demmler, J. Limpert, and A. Tünnermann, New J. Phys. **16**, 033022 (2014).

[29] S. Hädrich, J. Rothhardt, M. Krebs, S. Demmler, A. Klenke, A. Tünnermann, and J. Limpert, J. Phys. B **49**, 172002 (2016).

[30] C. M. Heyl *et al.*, Optica **3**, 75 (2016).

[31] E. J. Takahashi, P. Lan, O. D. Mücke, Y. Nabekawa, and K. Midorikawa, Nat. Commun. **4**, 2691 (2013).

[32] L. E. Chipperfield, J. S. Robinson, J. W. G. Tisch, and J. P. Marangos, Phys. Rev. Lett. **102**, 063003 (2009).

[33] F. Brizuela *et al.*, Sci. Rep. **3**, 1410 (2013).

[34] P. Wei, J. Miao, Z. Zeng, C. Li, X. Ge, R. Li, and Z. Xu, Phys. Rev. Lett. **110**, 233903 (2013).

[35] S.-W. Huang *et al.*, Nat. Photon. **5**, 475 (2011).

[36] A. Wirth *et al.*, Science **334**, 195 (2011).

[37] S. Haessler, T. Balčiunas, G. Fan, G. Andriukaitis, A. Pugžlys, A. Baltuška, T. Witting, R. Squibb, A. Zaïr, J. W. G. Tisch, J. P. Marangos, and L. E. Chipperfield, Phys. Rev. X **4**, 021028 (2014).

[38] C. Jin and C. D. Lin, Chin. Phys. B **25**, 094213 (2016).

[39] C. Jin, G. Wang, H. Wei, A.-T. Le, and C. D. Lin, Nat. Commun. **5**, 4003 (2014).

[40] C. Jin, G. J. Stein, K.-H. Hong, and C. D. Lin, Phys. Rev. Lett. **115**, 043901 (2015).

[41] C. Jin, K.-H. Hong, and C. D. Lin, Sci. Rep. **6**, 38165 (2016).

[42] F. Böhle *et al.*, Laser Phys. Lett. **11**, 095401 (2014).

[43] K. Cassou, S. Daboussi, O. Hort, O. Guilbaud, D. Descamps, S. Petit, E. Mével, E. Constant, and S. Kazamias, Opt. Lett. **39**, 3770 (2014).

[44] S. J. Goh, J. Reinink, Y. Tao, P. J. M. van der Slot, H. J. M. Bastiaens, J. L. Herek, S. G. Biedron, S. V. Milton, and K.-J. Boller, Opt. Express **24**, 1604 (2016).

[45] E. J. Takahashi, T. Kanai, K. L. Ishikawa, Y. Nabekawa, and K. Midorikawa, Phys. Rev. Lett. **101**, 253901 (2008).

[46] J. Yao, H. Xiong, H. Xu, Y. X. Fu, B. Zeng, W. Chu, Y. Cheng, Z. Z. Xu, X. J. Liu, and J. Chen, Sci. China Phys. Mech. Astron. **53**, 1054 (2010).

[47] P. Ye, H. Teng, X.-K. He, S.-Y. Zhong, L.-F. Wang, M.-J. Zhan, W. Zhang, C.-X. Yun, and Z.-Y. Wei, Phys. Rev. A **90**, 063808 (2014).

[48] A. T. Le, R. R. Lucchese, S. Tonzani, T. Morishita, and C. D. Lin, Phys. Rev. A **80**, 013401 (2009).

[49] C. Jin, A. T. Le, and C. D. Lin, Phys. Rev. A **83**, 023411 (2011).

[50] A. Dubrouil, O. Hort, F. Catoire, D. Descamps, S. Petit, E. Mével, V. V. Strelkov, and E. Constant, Nat. Commun. **5**, 4637 (2014).

[51] H.-W. Sun, P.-C. Huang, Y.-H. Tzeng, R.-T. Huang, C. D. Lin, C. Jin, and M.-C. Chen, Optica (to be published).